

Ca₆[Cr₂N₆]H, the First Quaternary Nitride–HydrideMark S. Bailey, Mark N. Obrovac,[†] Emilie Baillet,[‡] Thomas K. Reynolds, David B. Zax, and Francis J. DiSalvo*

Department of Chemistry and Chemical Biology, Cornell University, Ithaca, New York 14853

Received March 26, 2003

The novel quaternary nitride–hydride Ca₆[Cr₂N₆]H was synthesized at 1000 °C in sealed niobium or stainless steel tubes. It crystallizes in the space group $R\bar{3}$ (No. 148, $Z = 3$) with lattice constants (Å) $a = 9.0042(2)$ and $c = 9.1898(3)$ and contains the complex anion [Cr₂N₆]¹¹⁻ with a short chromium–chromium bond length of 2.26 Å. To our knowledge, this is the first example of a non-nitrogen-bridged chromium–chromium dimer in an extended structure compound. Magnetic susceptibility measurements reveal the compound to be paramagnetic at room temperature and with a broad antiferromagnetic ordering centered around 55 K.

Introduction

Nitride–hydrides are few and far between. In such compounds, both nitrogen and hydrogen are formally anionic and no nitrogen–hydrogen bonds are observed. Only four of these compounds are well described in the literature. These are the nitride–hydrides of lithium¹ and the alkaline earth (Ae) metals calcium,^{2–4} strontium,³ and barium.³ Li₄NH crystallizes in a variant of the Li₂O structure type while Ca₂N(H/D) adopts an ordered variant of the rock salt structure type. Both strontium and barium nitride–hydride crystallize in the *anti-α*-NaFeO₂ structure type. In all three of the Ae nitride–hydrides the Ae cations adopt a close-packed arrangement. The holes are fully occupied in an ordered arrangement of N³⁻ and H¹⁻ so that, for example, in Sr₂NH the layer sequence is –H–Sr–N–Sr–H–. Interestingly, only the amides (nitrogen–hydrogen bonded) of magnesium⁵ and beryllium⁶ are known and it is not clear whether attempts have been made to synthesize their nitride–hydrides. References to nitride–hydrides of elements beyond the s-block do exist. Titanium,⁷ zirconium,⁸ and niobium⁹ nitride–hydride are mentioned in the Russian literature, but

it appears that these three compounds are all somewhat deficient in nitrogen and/or hydrogen. For example, Ti₂N_{0.8}H_{0.42} consists of hcp titanium with nitrogen filling the octahedral holes (two sites, 77% and 3% occupied) and hydrogen the tetrahedral holes (21% occupied). The only other mention of nitride–hydrides is in reference to silicon nitride–hydride thin films,¹⁰ but in these compounds there are nitrogen–hydrogen bonds. To our knowledge there are no examples of quaternary nitride–hydrides.

Often the structures of transition metal (M) ternary nitrides are described in terms of isolated or condensed nitridometalate species, M_xN_y^{z-}, that are surrounded by electropositive cations. The nitrogen anions are usually 6-fold coordinate to M and/or the electropositive metal(s), often alkaline earth metals.¹¹ For example, sheets of edge- and corner-sharing TiN₄ tetrahedra are found in SrTiN₂¹² while infinite –Ni–N–Ni– chains are found in CaNiN.¹³ Smaller nitridometalate motifs can also be found, e.g. the finite bent chains of [Cu₂N₃]⁷⁻ in Sr₆Cu₃N₅¹⁴ or the edge-sharing pairs of trigonal planar units, [Fe₂N₄]⁸⁻, in Ca₂[FeN₂].¹⁵ Some of these

* To whom correspondence should be addressed. E-mail: fjd3@cornell.edu.

[†] Current address: 3M Electronics & Inorganics Technology Center, 3M Center, 209-2C-26, St Paul, MN 55144-1000.[‡] Current address: Carnegie Mellon University, Materials Science and Engineering Department, Wean Hall, 5000 Forbes Ave, Pittsburgh, PA 15213.

- (1) Marx, R. Z. *Anorg. Allg. Chem.* **1997**, *623*, 1912–1916.
- (2) Sichla, T.; Jacobs, H. *Eur. J. Solid State Inorg. Chem.* **1995**, *32*, 49–56.
- (3) Jacobs, H.; Niewa, R.; Sichla, T.; Tenten, A.; Zachwieja, U. *J. Alloys Compd.* **1997**, *246*, 91–100.
- (4) Reckeweg, O.; DiSalvo, F. J. *Solid State Sci.* **2002**, *4*, 575–584.
- (5) Jacobs, H. Z. *Anorg. Allg. Chem.* **1971**, *382*, 97–109.
- (6) Jacobs, H. Z. *Anorg. Allg. Chem.* **1976**, *427*, 1–8.

- (7) Khidirov, I.; Kurbonov, I.; Mukhtarova, N. N. *Kristallografiya* **1996**, *41*, 450–456.
- (8) Khidirov, I.; Karimov, I.; Em, V. T.; Loryan, V. E. *Izv. Akad. Nauk SSSR, Neorg. Mater.* **1986**, *22* (4), 609–612.
- (9) Nemoshkalenko, V. V.; Kindrat, M. M.; Krivitskii, V. P.; Mamko, B. P. *Zh. Neorg. Khim.* **1983**, *28* (2), 295–298.
- (10) Smith, D. L.; Alimonda, A. S.; von Preissig, F. J. *J. Vac. Sci. Technol.* **1990**, *B8*, 551–557.
- (11) Niewa, R.; DiSalvo, F. J. *Chem. Mater.* **1998**, *10*, 2733–2752.
- (12) Gregory, D. H.; Barker, M. G.; Edwards, P. P.; Siddons, D. J. *Inorg. Chem.* **1998**, *37*, 3775–3778.
- (13) Chern, M. Y.; DiSalvo, F. J. *J. Solid State Chem.* **1990**, *88*, 459–464.
- (14) DiSalvo, F. J.; Trail, S. S.; Yamane, H.; Brese, N. E. *J. Alloys Compd.* **1997**, *255*, 122–129.

nitridometalate units contain M–M bonding, but in every case the transition metals are also bridged by nitrogen. The only example of a nonbridged M–M bond in a nitridometalate is in the recently reported compound $\text{Li}_6\text{Ca}_2[\text{Mn}_2\text{N}_6]$,¹⁶ which contains the ethane-like anion $[\text{Mn}_2\text{N}_6]^{10-}$. The manganese–manganese separation within these dimers is 2.36 Å, which is approximately 0.35 Å shorter than in elemental manganese.

A variety of oxidation states for chromium have been observed in its ternary and higher nitrides. The compounds Ae_3CrN_3 (Ae = Ca,¹⁷ Sr,¹⁸ Ba¹⁸) contain Cr(III) while Cr(V) is found in $\text{Li}_4\text{Sr}_2[\text{Cr}_2\text{N}_6]$,¹⁹ $\text{Ae}_4[\text{Cr}_2\text{N}_6]$ ²⁰ (Ae = Ca and Sr), and $\text{Ba}_5[\text{CrN}_4]\text{N}$.²¹ A fully oxidized Cr(VI) exists within the compound $\text{Li}_{15}\text{Cr}_2\text{N}_9$,²² but to our knowledge, there are no examples of Cr(IV) nor of mixed-valence chromium atoms within compounds containing easily identifiable oxidation states i.e. not including mixed transition metal nitrides such as $\text{V}_{1-x}\text{Cr}_x\text{N}$,²³ an alloy of the rocksalt structure binary compounds VN and CrN, and not including intermetallic subnitrides such as Cr_2GaN .²⁴ Some examples of mixed-valent chromium are found in solid state oxides. Both Cr(III) and Cr(VI) formally exist in the compounds $\text{La}_{1-x}\text{Ae}_x\text{CrO}_3$ (Ae = Ca²⁵ and Sr²⁶) and $\text{Sr}_{4.5}\text{Cr}_{2.5}\text{O}_9$ ²⁷ while in $\text{Nd}_{1-x}\text{Ca}_x\text{CrO}_4$ ²⁸ ($x = 0.02\text{--}0.2$) both Cr(V) and Cr(VI) are expected.

This paper reports the synthesis and characterization of $\text{Ca}_6[\text{Cr}_2\text{N}_6]\text{H}$, a compound that adds to all three of the previously described areas. It is the first example of a quaternary nitride–hydride and provides the first report of a mixed-valence chromium nitride. Furthermore, one of the formally accessed valences must be Cr(IV), which is bonded to a Cr(III) in only the second example of a non-nitrogen-bridged M–M bond in nitrides. It is also the first example of a chromium–chromium dimer in an extended structure (i.e. nonmolecular) compound.

Experimental Section

All sample manipulations were performed in an argon-filled glovebox. Chromium nitride (CrN) was prepared by heating Cr powder (Fisher 99%) in flowing ammonia at 800 °C for 24 h. The

resulting powder (a mixture of Cr_2N and CrN) was reground and heated under the same conditions for an additional 4 days. This yielded phase pure CrN as verified by powder X-ray diffraction (XRD). Calcium nitride was prepared by heating a calcium rod (ESPI, 99%) in a nitrogen stream for 2 days at 1000 °C. Titanium wire and calcium metal powder were placed just before the calcium rod in the nitrogen stream to remove trace water and oxygen impurities from the nitrogen. The calcium nitride was subsequently ground to a fine powder. Only peaks from Ca_3N_2 were present in its powder XRD pattern. Ethylenediamine (Aldrich, 99%) was dried 30 days over molecular sieves and then vacuum distilled prior to use. Li_3N (Alfa Aesar, 99.5%) and CaH_2 (Aldrich, 99.5+%) were used as obtained.

Initially, $\text{Ca}_6[\text{Cr}_2\text{N}_6]\text{H}$ was synthesized as X-ray-sized crystals by grinding 139.3 mg of Li_3N (4 mmol) with 296.5 mg of Ca_3N_2 (2 mmol) and 198.0 mg of CrN (1 mmol) which provided an elemental ratio Li:N:Ca:Cr of 12:9:6:1. The powdered mixture was heated in a sealed niobium tube at 1000 °C for 3 days and then cooled slowly to 500 °C over 2 days. A few small black irregularly shaped crystals were embedded in a soft, silvery metallic matrix that could be washed away with ethylenediamine while leaving the crystals unaffected. Microprobe analysis (JEOL 8900) indicated a Ca:Cr ratio of $2.9 \pm 0.1:1$, the presence of nitrogen, and the absence of carbon and oxygen. To prevent decomposition or oxygen contamination of the samples, they were transferred from an argon-filled glovebox to the microprobe in a specially designed portable antechamber that avoids any air exposure while transferring the sample to the microprobe.²⁹

Samples of these crystals were removed from the glovebox in polybutene oil for optical analysis and single-crystal selection. The crystals, when loaded onto the goniometer, were within a cold nitrogen stream that froze the polybutene oil thus keeping the crystals stationary and protected from oxygen and moisture in the air. Data were collected on a Bruker Smart CCD (φ and ω scans) equipped with a graphite monochromator and using Mo $\text{K}\alpha$ ($\lambda = 0.71073$ Å) radiation. Initial single-crystal diffraction studies suggested a composition of Ca_3CrN_3 . This was very surprising since the previously reported structure of the burgundy compound Ca_3CrN_3 ¹⁷ has a very different structure that contains isolated CrN_3^{6-} units. The structure of the new black crystals indicated an excess electron density at the center of a distorted Ca_6 octahedron. This electron density was consistent with that expected for a hydride, yielding a composition $\text{Ca}_6[\text{Cr}_2\text{N}_6]\text{H}$. We hypothesized that the hydrogen could have originated either from the niobium tube or from the commercial lithium nitride powder.

A bulk powder sample of $\text{Ca}_6[\text{Cr}_2\text{N}_6]\text{H}$ was made from a mixture of 100 mg of CrN, 225 mg of Ca_3N_2 , and 32 mg of CaH_2 which provided the calcium, chromium, nitrogen, and hydrogen in the molar ratios of 3.5:1:3:1, i.e. with an excess of calcium and hydrogen. This mixture was ground-up, pressed into a pellet, and sealed in a stainless steel tube under ~ 1 atm argon with a Centorr Associates arc furnace. This container was itself sealed inside a fused silica tube to be protected from subsequent oxidation. A control reaction was also carried out between 98 mg of CrN and 262 mg of Ca_3N_2 (molar ratios Ca:Cr:N = 3.6:1:3.4) which was prepared for heating in an identical manner. Both tubes were placed into the same furnace, heated to 1000 °C in 15 h, and remained at that temperature for 100 h at which point the furnace switched off and cooled naturally. When both tubes were opened, they revealed a black powder. The powder XRD data from these samples were

- (15) Höhn, P.; Kniep, R. *Z. Naturforsch.* **1992**, *47b*, 477–481.
 (16) Hochrein, O.; Grin, Y.; Kniep, R. *Angew. Chem., Int. Ed.* **1998**, *37* (11), 1582–1585.
 (17) Vennos, D. A.; Badding, M. E.; DiSalvo, F. J. *Inorg. Chem.* **1990**, *29*, 4059–4062.
 (18) Barker, M. G.; Begley, M. J.; Edwards, P. P.; Gregory, D. H.; Smith, S. E. *J. Chem. Soc., Dalton Trans.* **1996**, *1*, 1–5.
 (19) Hochrein, O.; Kohout, M.; Schnelle, W.; Kniep, R. *Z. Anorg. Allg. Chem.* **2002**, *628*, 2738–2743.
 (20) Bailey, M. S.; DiSalvo, F. J. *J. Chem. Soc., Dalton Trans.* **2003**, *12*, 2621–2625.
 (21) Tennstedt, A.; Kniep, R.; Hüber, M.; Haase, W. *Z. Anorg. Allg. Chem.* **1995**, *621*, 511–515.
 (22) Gudat, A.; Haag, S.; Kniep, R.; Rabenau, A. *Z. Naturforsch.* **1990**, *45b*, 111–120.
 (23) Eddine, M. N.; Bertaut, E. F.; Roubin, M.; Pâris, J. *Acta Crystallogr.* **1977**, *B33*, 3010–3013.
 (24) Beckmann, O.; Boller, H.; Nowotny, H.; Benesovsky, F. *Monatsh. Chem.* **1969**, *100*, 1465–1470.
 (25) Liu, X.; Su, W.; Lu, Z. *J. Phys. Chem. Solids* **2001**, *62*, 1919–1921.
 (26) Liu, X.; Su, W.; Lu, Z.; Liu, J.; Pei, L.; Liu, W.; He, L. *J. Alloys Compd.* **2000**, *305*, 21–23.
 (27) Pelloquin, D.; Wahl, A.; Masset, A. C.; Maignan, A.; Michel, C.; Raveau, B. *J. Solid State Chem.* **2000**, *154*, 375–383.
 (28) Aoki, Y.; Konno, H. *J. Solid State Chem.* **2001**, *156*, 370–378.

- (29) Ehrlich, G. M. The synthesis of linked metal clusters. Ph.D. Thesis, Cornell University, Ithaca, NY, 1995.

collected with a Scintag XRD 2000 diffractometer using Cu K α radiation, and to exclude air and moisture during the scan, the samples were covered with a Mylar film.

Results and Discussion

The single-crystal synthesis of Ca₆[Cr₂N₆]H was completed before the powder experiments. As previously mentioned, we initially assumed that another polymorph of Ca₃CrN₃ had been synthesized, in which the [CrN₃]⁶⁻ units had condensed into [Cr₂N₆]¹²⁻ dimers. This would have represented the first example of a Cr(III)–Cr(III) bond.³⁰ Doubts about the crystal structure of this new polymorph began to emerge when it was noted that there was considerable excess electron density at the center of a Ca₆ distorted octahedron. The distance, 2.65 Å, from the center of these octahedra to their vertices was also consistent with possible hydride occupancy. This initiated the powder syntheses explained in the Experimental Section; i.e., reactions with and without hydrogen were carried out. Both these reactions yielded a black powder. The peak positions and degree of crystallinity exhibited in the powder XRD patterns from these two samples were distinctly different. Those from the hydrogen-containing reaction were also sharper and more intense. The program TREOR³¹ was used to index most of these peaks to a hexagonal cell with $a = 9.013$ Å and $c = 9.196$ Å. Several weak peaks (<10% of the strongest peaks of the main phase) were also observed but could not be indexed to known phases. These may arise from the slightly nonstoichiometric mixture that was used in the powder synthesis. These hexagonal lattice parameters are in close agreement with those obtained from the single-crystal refinement; cf. Table 1. The sample without hydrogen did not display any X-ray diffraction peaks that could be indexed on the hexagonal cell, and we could not definitely identify the phases present because most of the peaks were weak and broad.

Microprobe analysis of the crystals confirmed that the only heavy elements ($Z \geq 6$) present were calcium, chromium, and nitrogen. Analysis of the coexisting soft, silvery metallic product gave no signal in the microprobe. The metal was found to be soluble in ethylenediamine, giving a strongly colored blue solution, confirming that the metal was primarily lithium, which would not be visible in the microprobe.

All single-crystal data sets were consistent with hexagonal symmetry and unit cell parameters of approximately $a = 9.00$ Å and $c = 9.19$ Å. Systematic extinctions led to the space groups $R\bar{3}$ (No. 148) or $R3$ (No. 146). The one of higher symmetry led to an acceptable refinement. The crystal structure was determined using the SHELXTL v. 5.1 software package,³² and all non-hydrogen atoms were found by direct methods. Following the refinements of calcium, chromium, and nitrogen, residual electron density ($3.4 \text{ e}^-/\text{Å}^3$) was apparent at the 3a special position (0, 0, 0). This position is

Table 1. Crystal Data and Structure Refinement Details of Ca₆[Cr₂N₆]H^a

temp	173(2) K
wavelength	0.710 73 Å
monochromator	graphite
cryst system	rhombohedral
space group	$R\bar{3}$
unit cell dimens	$a = 9.0042(2)$ Å; $\alpha = 90^\circ$ $b = 9.0042(2)$ Å; $\beta = 90^\circ$ $c = 9.1898(3)$ Å; $\gamma = 120^\circ$
V	645.24(3) Å ³
Z	3
$D(\text{calcd})$	3.316 Mg/m ³
abs coeff	6.053 mm ⁻¹
abs corr	SADABS
crystal size	0.20 × 0.10 × 0.10 mm ³
θ range for data collcn	3.43–41.03°
index ranges	$-13 \leq h \leq 12$, $-15 \leq k \leq 9$, $-12 \leq l \leq 16$
reflcn collcd	3591
indpdt reflcn	884 [R(int) = 0.0351]
max and min transm	0.5828 and 0.3773
refinement method	full-matrix least squares on F^2
data/restraints/params	884/0/24
goodness-of-fit on F^2	1.137
final R indices [$I > 2\sigma(I)$]	R1 = 0.0370, wR2 = 0.0799
R indices (all data)	R1 = 0.0430, wR2 = 0.0822
extinction coeff	0.0171(13)
largest diff peak and hole	0.928 and $-1.014 \text{ e}^-/\text{Å}^3$

^a These details were obtained from refinement cycles with hydrogen present with a site occupancy factor (sof) of 200%. The calculated density and absorption coefficient are as obtained with the sof = 100%.

at the center of a distorted calcium octahedron, a very attractive site for a hydride. To model hydride occupancy, a hydrogen atom was placed at this site but with its site occupancy factor (sof) set to 200%. Refinements of this model lead to a very small reduction in R1 from 0.0384 to 0.0370, but the largest diffraction peak and hole decreased to 0.928 and $-1.014 \text{ e}^-/\text{Å}^3$. These are both close (<1.0 Å) to the calcium atom and result from the Fourier series truncation of the diffraction data to $2\theta < 42^\circ$. Placing any atom with $Z \geq 3$ at this site, with a sof of 100%, resulted in the generation of very large thermal parameters for the atom. This indicates that these heavier elements contain too many electrons to correctly model this Fourier peak. The hydride site was also modeled as containing nitrogen with partial occupancy. Changing from a doubly occupied hydrogen atom (to model hydride) to a nitrogen atom whose occupancy was allowed to vary freely had no noticeable effect on the R1 value or residual electron densities. The refined occupancy fell to 18% with a thermal parameter whose magnitude was four times that of the fully occupied nitrogen sites. From X-ray data alone we cannot be certain what atom occupies this site, if partial occupancy is possible. As we argue below, however, the evidence strongly indicates that the site is occupied with hydride anions. The details of the final refinement, which included a doubly occupied hydrogen site (i.e. a model of H⁻), are shown in Table 1. The density and absorption coefficient are those found from a refinement cycle with a singly occupied hydrogen site. No additional symmetry was found by ADDSYM.³³ The atomic positions were standardized with STRUCTURE TIDY³⁴ and are shown in Table 2. The anisotropic thermal parameters of the non-

(30) Cotton, F. A.; Walton, R. A. *Multiple Bonds Between Metal Atoms*, 2nd ed.; Clarendon Press and Oxford University Press: Oxford, U.K., New York, 1993.

(31) Werner, P.-E.; Eriksson, L.; Westdahl, M. *J. Appl. Crystallogr.* **1985**, *18*, 367–370.

(32) Sheldrick, G. M. *SHELXTL 5.1*; Bruker Analytical X-ray Instruments; Madison, WI, 1998.

(33) Farrugia, L. J. *J. Appl. Crystallogr.* **1999**, *32*, 837–838.

(34) Gelato, L. M.; Parthé, E. *J. Appl. Crystallogr.* **1987**, *20*, 139–143.

Table 2. Atomic Coordinates as Fractions of the Unit Cell Parameters and Equivalent Isotropic Displacement Parameters ($\text{\AA}^2 \times 10^3$) That Were Produced from Refinements with a Doubly Occupied Hydrogen Site

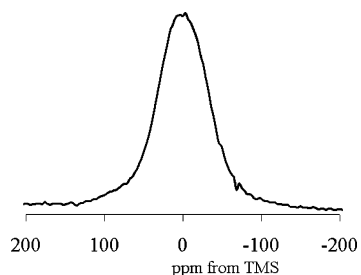
atom	Wyckoff site	x/a	y/b	z/c	U_{eq}^a
Ca	18f	0.0544(1)	0.2682(1)	0.1587(1)	5(1)
N	18f	0.2123(2)	0.1676(2)	0.3197(2)	5(1)
Cr	6c	0	0	0.3772(1)	3(1)
H	3a	0	0	0	4(7)

^a U_{eq} is defined as one-third the trace of the orthogonalized U_{ij} tensor.

Table 3. Anisotropic Displacement Parameters ($\text{\AA}^2 \times 10^3$) Obtained from the Refinement of $\text{Ca}_6[\text{Cr}_2\text{N}_6]\text{H}$ with a Doubly Occupied Hydrogen Site^a

atom	U^{11}	U^{22}	U^{33}	U^{23}	U^{13}	U^{12}
Ca	5(1)	7(1)	4(1)	2(1)	1(1)	3(1)
N	5(1)	6(1)	5(1)	0(1)	0(1)	3(1)
Cr	3(1)	3(1)	3(1)	0	0	2(1)

^a The anisotropic displacement factor exponent takes the following form: $-2\pi[h^2a^*2U^{11} + \dots + 2hka^*b^*U^{12}]$.


Figure 1. Proton NMR signal. The broad peak is centered at approximately -24 ppm, and the spectral width is 120 kHz.

hydrogen atoms are shown in Table 3. All the details shown in these tables were derived from refinement cycles with a doubly occupied hydrogen site. While we were now confident that the new compound was indeed a nitride–hydride, the presence of hydrogen should be verified by other means, since the X-ray scattering power of hydride is very low compared to that of the other elements present.

NMR Measurements. In an effort to further verify the presence of hydrogen, solid-state proton NMR experiments were taken from the nearly single-phase powder sample, which was sealed in an evacuated NMR tube. Measurements were taken in a 7.05 T wide-bore superconducting magnet equipped with home-built probes and a broad-band, pulsed Fourier transform spectrometer. A blank was run initially to ensure that the absorption came only from the sample. The spectrum of the sample is shown in Figure 1. A broad absorption, centered at approximately -24 ppm relative to tetramethylsilane (TMS), is clearly evident. Such a large upfield shift is consistent with a paramagnetically shifted hydride. Furthermore, the relaxation time (T_1) is approximately 100 ms, which is almost 2 orders of magnitude shorter than what is typically found in hard inorganic materials with low ^1H densities, and is similarly consistent with hydrogen atoms in close contact with paramagnetic electrons. All this indicates that the signal is coming from the bulk paramagnetic sample, *vide infra*, and not the low level of impurities that are present; i.e., according to previously published studies, this relaxation time is much too short to arise from

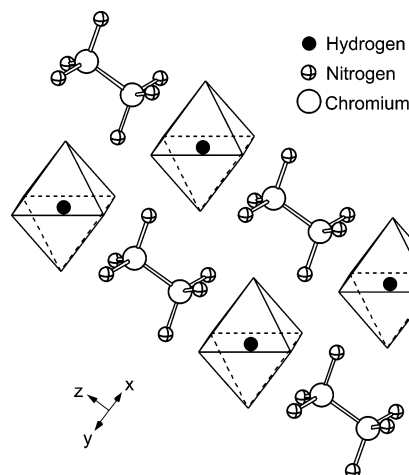

Figure 2. Structure of $\text{Ca}_6[\text{Cr}_2\text{N}_6]\text{H}$. The calcium atoms are at the apices of the octahedra.

Table 4. Interatomic Distances Less Than 3 \AA in $\text{Ca}_6[\text{Cr}_2\text{N}_6]\text{H}$

atoms	no.	dist/ \AA	atoms	no.	dist/ \AA
Cr–N	3	1.8236 (15)	Ca–H	6	2.6491(4)
Cr–Cr	1	2.2573 (8)	Cr–Ca	3	2.9868(4)
Ca–N	5	2.471(1)–2.535(1)			

Table 5. Selected Bond Angles (deg) around the Atoms in $\text{Ca}_6[\text{Cr}_2\text{N}_6]\text{H}$

N–Cr–N	111.96(4) \times 3	Ca–H–Ca	87.407(1)–92.593(2) \times 12
N–Cr–Cr	106.85(5) \times 3	N–Ca–H	82.84(3)–88.92 \times 4
Cr–N–Ca	85.47(6)–101.60(6) \times 4	N–Ca–N	74.30(7)–100.20(1) \times 8
Ca–N–Ca	78.75(4)–99.84(5) \times 8		

any remaining calcium hydride.³⁵ This result, coupled with our failure to synthesize a bulk powder sample of the same structure without hydrogen, is clear evidence that the compound is a nitride–hydride rather than a pure nitride.

Structure Description. As shown in Figure 2, the structure can be described as a packing of two building blocks, slightly distorted Ca_6H octahedra and Cr_2N_6 ethane-like units. These stack alternately to form chains that run parallel to the z axis. These chains then pack in the xy plane but are offset from one another in z , consistent with the presence of an inversion center. In each individual chain, the nitrogen atoms are situated such that they are staggered in the Cr_2N_6 unit and to the three calcium atoms that form the nearest face of the Ca_6N octahedra. Important interatomic distances and bond angles are shown in Tables 4 and 5, respectively.

The calcium hydrogen distances in the Ca_6H unit are 2.65 \AA , which is identical to those observed in the compound $\text{Ca}_2\text{-ND}$,² where the deuterium also resides in the center of a Ca_6 octahedron. Calcium deuteride, CaD_2 ,³⁶ presents two different distorted environments for the deuterium, *viz.* pseudotetrahedral and distorted square pyramidal. The bond distances between the calcium atoms and the 4- and 5-fold deuterium atoms range from 2.16 to 2.5 and 2.31 to 2.8 \AA , respectively. This trend is to be expected because as the

(35) Andresen, A. F.; Maeland, A. J.; Slotfeldt-Ellingsen, D. *J. Solid State Chem.* **1977**, *20*, 93–101

(36) Sichla, T.; Jacobs, H. *Eur. J. Solid State Inorg. Chem.* **1996**, *33*, 453–461.

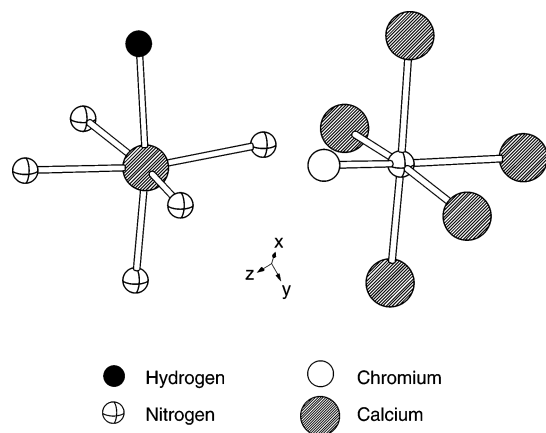


Figure 3. Local coordination environment of the calcium and nitrogen atoms.

coordination number decreases the degree of bonding between the central and apex atoms must increase to saturate the metal valence, hence the shorter bond distances.

Figure 3 shows the local environment of the nitrogen and calcium atoms in $\text{Ca}_6[\text{Cr}_2\text{N}_6]\text{H}$, and it can be seen that both are 6-fold coordinate. In both cases, the five bonds of the same type have lengths in the range 2.47–2.54 Å. Nitrogen also has one bond to chromium at a distance of 1.82 Å. Calcium completes its hexacoordination with a bond to hydrogen at a distance of 2.65 Å. Within the $[\text{Cr}_2\text{N}_6]^{11-}$ unit the chromium–chromium separation is 2.26 Å, which is approximately 0.25 Å shorter than in elemental chromium. There are no chromium-containing analogues to compare to, but this distance is 0.1 Å shorter than that between the manganese atoms in $\text{Li}_6\text{Ca}_2[\text{Mn}_2\text{N}_6]$.¹⁶ This may be due to the smaller combined formal charges and hence smaller Coulombic repulsion between a Cr(III) and a Cr(IV) compared to two Mn(IV). In molecular compounds, W(III)–W(III) and Mo(III)–Mo(III) bonding in a staggered ethane conformation is common.³⁷ Generally the bond lengths in these materials fall in the range of 2.167–2.30 Å and have a M–M–ligand angle of about 104°, which compares well to that observed for $\text{Ca}_6[\text{Cr}_2\text{N}_6]\text{H}$, despite the smaller size of the chromium ion. The type of ethane-style metal–metal bonding shown in the $[\text{N}_3\text{CrCrN}_3]^{11-}$ dumbbells has never been observed for any valence, or mixed valence, of chromium. In molecular compounds there are some examples of nonbridged chromium–chromium complexes, including $\text{Li}_4\text{Cr}_2(\text{C}_4\text{H}_8)_4 \cdot 4\text{H}_2\text{O}$.³⁰ Each chromium atom in this compound is Cr(II) and is chelated to two C_4H_8 ligands to create a unit of approximate D_{2d} symmetry. The Cr(II)–Cr(II) separation is only ~1.98 Å and is reported to be a quadruple chromium–chromium bond. This is in contrast to the C_{3v} symmetry and 2.26 Å metal–metal bond length exhibited by the $[\text{Cr}^{\text{III}}\text{Cr}^{\text{IV}}\text{N}_6]^{11-}$ ion of the title compound.

The bond valence sums and Madelung site potentials were calculated with the program EUTAX³⁸ and are shown in Table 6. The internal program values of the R_{ij} were used to calculate the bond valence sums. The cation–anion, anion–

Table 6. Calculated Bond Valence Sums and Madelung Potentials of $\text{Ca}_6[\text{Cr}_2\text{N}_6]\text{H}$ ^a

atom	bond valence sum	Madelung potential/V
Ca	1.99	–21.37
Cr	3.23	–36.38
N	2.96	32.57
H	0.66	9.86

^a Only chromium–nitrogen, calcium–nitrogen, and calcium–hydrogen interactions are used to calculate the total valence sums.

anion, and cation–cation R_{ij} values are as found in refs 38–40, respectively. The resulting bond valence sums of calcium and nitrogen are very close to the ideal values of 2 and 3. The value for hydrogen is a little low and for chromium a little high (based upon Cr(III)) but not so much as to court disbelief. The chromium bond valence sum is determined from the chromium–nitrogen interactions alone. A chromium–chromium bond valence of 1.19 is calculated from the inter-chromium distance of 2.26 Å. The Madelung potentials were determined by assigning ionic charges for all elements, and because there is only one crystallographically distinct chromium site, the oxidation state of chromium was assigned to be +3.5. The results are all in line with results typically found in most halides, oxides, and nitrides; i.e., the calculated values are approximately $(-10 \times \text{charge})$ V. Thus it can be seen that the value of +32 V for the nitrogen site strongly supports the elemental designation, being approximately 10 V larger than what would be expected for an oxygen site. The values for the hydrogen and chromium site are also in line with this expectation.

Magnetic Studies. The magnetic susceptibility of the same sample as used in the NMR studies was measured with a Quantum Design SQUID magnetometer in a 1 T field from 5 to 295 K. A M vs H curve was first measured at room temperature, which revealed a small ferromagnetic impurity in the sample. The contribution of this impurity to the measurements was subtracted by the method of Owen and Honda.⁴¹ The diamagnetic signal of the NMR tube could not be measured as it broke when attempts were made to remove the sample. As shown in Figure 4 the total susceptibility of the sample and the diamagnetic container is paramagnetic; i.e., it is clear that the sample itself is quite paramagnetic. It can be seen that above 100 K the paramagnetic susceptibility decreases with increasing temperature but below this there is a broad antiferromagnetic peak centered at around 55 K (see inset to Figure 4). The minimum and subsequent upward trend below 50 K is likely due to low levels of a paramagnetic impurity in the bulk of the sample. An attempt was made to fit the data above 100 K to the modified Curie–Weiss equation, $\chi = \chi_0 + C/(T + \Theta)$, but it resulted in a large value of $\Theta \sim 500$ K. Generally, one expects the Curie–Weiss expression to be valid only when $T \geq n\Theta$ for $n = 1.5$ or greater.⁴² However, if the data were

(37) Chisholm, M. H.; Cotton, F. A. *Acc. Chem. Res.* **1978**, *11*, 356–362.

(38) Brese, N. E.; O’Keeffe, M. *Acta Crystallogr.* **1991**, *B47*, 192–197.

(39) O’Keeffe, M.; Brese, N. E. *Acta Crystallogr.* **1992**, *B48*, 152–154.

(40) O’Keeffe, M.; Brese, N. E. *J. Am. Chem. Soc.* **1991**, *113*, 3226–3229.

(41) Selwood, P. W. *Magnetochemistry*, 2nd ed.; Interscience: New York, 1956; pp 351–352.

(42) Smart, J. S. *Effective Field Theories of Magnetism*; W. B. Saunders Co.: Philadelphia, PA, 1966.

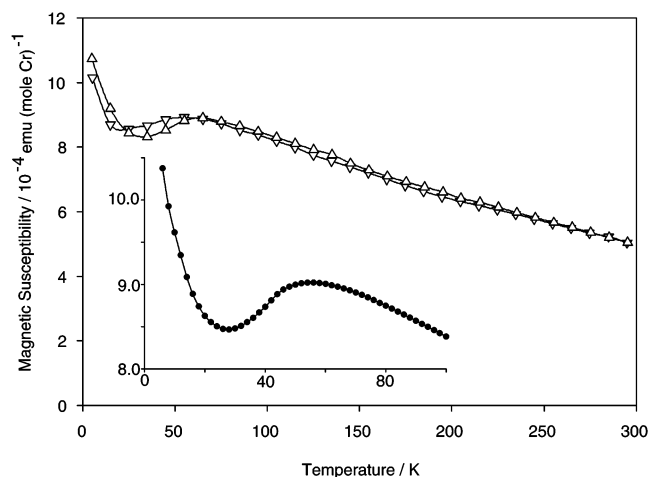


Figure 4. Temperature dependence of the magnetic susceptibility of $\text{Ca}_6[\text{Cr}_2\text{N}_6]\text{H}$. Upward pointing triangles indicate data taken on heating, and downward pointing triangles indicate data taken on cooling. The inset shows a higher density of data that were collected on a second cooling cycle through the antiferromagnetic transition region.

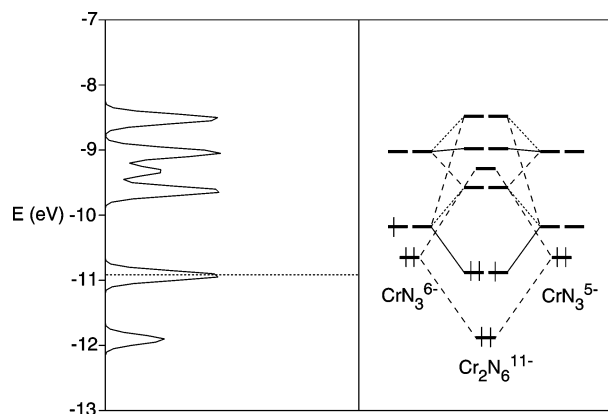


Figure 5. Density of states (DOS) of $\text{Ca}_6[\text{Cr}_2\text{N}_6]\text{H}$. For clarity the scale has been chosen so as to avoid the nitrogen- and calcium-derived levels in the DOS. The Fermi energy is indicated by the dotted line at -10.9 eV. Shown next to the DOS is the result of a molecular orbital calculation for two hypothetical CaN_3^{x-} moieties ($x = 5$ and 6) and the $[\text{Ca}_2\text{N}_6]^{11-}$ anion.

forced to fit the Curie–Weiss expression, then a value of $\mu_{\text{eff}} \approx 2.7 \mu_{\text{B}}/\text{mol}$ of Cr is obtained. This value is on the order of $3.87 \mu_{\text{B}}$ expected for high-spin Cr(III) or $2.83 \mu_{\text{B}}$ for Cr(IV).

Electronic Structure. Figure 5 shows the density of states (DOS) of $\text{Ca}_6[\text{Cr}_2\text{N}_6]\text{H}$ and the calculated molecular orbital diagram of an isolated, low-spin $[\text{Cr}_2\text{N}_6]^{11-}$ unit. These were calculated at the extended Hückel level with the program YAeHMOP⁴³ using Slater type orbitals with the program default values of the energies and exponents. The $[\text{Cr}_2\text{N}_6]^{11-}$ unit is formed by the interaction of two $[\text{CrN}_3]^{x-}$ fragments, one with $x = 5$ and one with $x = 6$. The molecular orbitals of these two units are calculated for the tetrahedral geometry that would arise from separating the dimer along the 3-fold symmetry axis, and it can be seen that the union of these two fragments has a large stabilizing effect on their valence levels. The filling of these valence orbitals is determined by electron–electron repulsion energies. Interestingly, Ca_3CrN_3 ,

which contains Cr(III) in a planar C_{2v} CrN_3^{6-} unit,¹⁷ contains low-spin chromium ($S = 1/2$). This pairing of the d electrons is thought to be due to a lowering of the electron–electron repulsion through valence orbital mixing that results from the strong π -donor interaction with the nitrido ligands.⁴⁴ The electron occupancy of the orbitals in Figure 5 is shown for the low-spin case (5 3d electrons). This arrangement would result in an average moment/chromium of $1.73/2^{1/2} = 1.22 \mu_{\text{B}}$. However, this would also result in a chromium–chromium bond order of 2.5, well above the 1.2 calculated by EUTAX. In the high-spin case (each orbital singly occupied) the bond order would be 0.5. The most likely case is one of intermediate spin, with the lowest orbital doubly occupied and the remaining orbitals singly occupied; i.e., $S = 3/2$ per dimer resulting in a net spin per chromium of $3.87/2^{1/2} = 2.74 \mu_{\text{B}}$. This value is surprisingly close to that fortuitously obtained from the “forced” Curie–Weiss fit. The bond order would be 1.5, not too different from the value of 1.2 obtained from EUTAX.

In terms of the Robin and Day⁴⁵ classification of mixed valence compounds, the fact that both the Cr(III) and Cr(IV) atoms are crystallographically identical leads to a class III assignment. Furthermore, as the metal centers form small, polynuclear clusters, it is more accurate to classify it as type III-A; i.e., there is no intercluster orbital overlap. This assignment is supported by the narrow nature of the bands in the calculated DOS (Figure 5).

Figure 5 may also explain why this type of metal–metal bonding has been observed for Mn^{4+} in $\text{Li}_6\text{Ca}_2[\text{Mn}_2\text{N}_6]$ ¹⁶ but not for Mn^{3+} in Ca_3MnN_3 ,⁴⁶ since Mn^{3+} – Mn^{3+} bonding in the latter would result in more electrons being placed in strongly antibonding orbitals (the number of antibonding orbitals occupied would depend on the spin configuration). However, metal–metal bonding may also be possible for transition metals such as vanadium that have fewer valence electrons. The quaternary nitride–hydride phase diagram of vanadium should be investigated further for evidence of phases that contain strong, nonbridged metal–metal bonds. Metal–metal bonding would likely also be present in the other alkaline earth metal analogues of $\text{Ca}_6[\text{Cr}_2\text{N}_6]\text{H}$.

Conclusion

The first quaternary chromium nitride–hydride has been synthesized. It contains both Cr(III) and Cr(IV), which are bonded to each other with only the second example of a direct metal–metal bond in nitrides. The compound is paramagnetic at room temperature with a weak antiferromagnetic transition centered around 55 K.

Acknowledgment. This work was supported by NSF Grant No. DMR-9805719. We thank Dr. Emil Lobkovsky for help with the single-crystal data collection and structure solution and Mr. John Hunt for help with the SEM micro-

(43) Landrum, G. A.; Glassey, W. YAeHMOP: Yet Another extended Hückel Molecular Orbital Package. YAeHMOP is freely available at <http://sourceforge.net/projects/yaehmop>.

(44) Alvarez, S. *Coord. Chem. Rev.* **1999**, *193–195*, 13–41.

(45) Robin, M. B.; Day, P. *Adv. Inorg. Chem. Radiochem.* **1967**, *10*, 247–422.

(46) Tennstedt, A.; Röhr, C.; Kniep, R. *Z. Naturforsch.* **1993**, *48b*, 1831–1834.

probe. The microprobe is supported by the Cornell Center for Materials Research Shared Experimental Facilities, funded through the National Science Foundation Materials Research Science and Engineering Program (Grant DMR-0079992).

Supporting Information Available: Crystallographic data in CIF format. This material is available free of charge via the Internet at <http://pubs.acs.org>.

IC0343206